

Characterization of Prepreg-Based Discontinuous Carbon Fiber/Epoxy Systems

PAOLO FERABOLI,* ELOF PEITSO, FRANCESCO DELEO AND TYLER CLEVELAND

*Aeronautics and Astronautics, University of Washington
Box 352400, Seattle, WA 98195-2400, USA*

PATRICK B. STICKLER

787 Technology Integration, Boeing Commercial Airplanes

ABSTRACT: This paper quantifies the elastic behavior and failure response of discontinuous carbon fiber/ epoxy laminates produced by compression molding of randomly oriented preimpregnated unidirectional tape. Flat plates have been successfully molded using manually prepared prepreg charges, and showed a satisfactory degree of randomization. Complex relationships between reinforcement aspect ratio and tensile, compressive, and flexural moduli and strengths are observed. For this particular material system, failure is a matrix-dominated event, with little or no fiber breakage, and it promotes relatively high variation in the measured properties. The high-volume carbon fiber content, combined with an aerospace-qualified epoxy resin, opens up opportunities for more aircraft parts to be made of composite materials, particularly for stiffness-critical components where discontinuous fibers offer performance similar to the continuous quasi-isotropic value.

KEY WORDS: short fiber, discontinuous fiber, carbon fibers.

INTRODUCTION

AIRFRAME COMPONENTS FABRICATED from composite materials have traditionally been a costly alternative to aluminum construction. The primary challenge that the aerospace industry faced leading up to the 787 was to fully obtain the performance benefits of composite materials while dramatically lowering production costs [1,2]. Recent composite technology research and development efforts have focused on new low-cost material product forms, and automated processes that can markedly increase production efficiencies. For example, efficient automated tape laying techniques have been developed in the last five years for manufacturing the integrally stiffened fuselage sections, such as the one developed by Boeing during the NASA-funded ATCAS Program [3]. Other examples of non-autoclave material forms used in that effort were the circumferential frames and the window frames, manufactured via resin infusion of textile preforms, a technique that enables the manufacturing of high-volume components at rapid rates and low recurring costs [3].

In components exhibiting fully three-dimensional geometry, where the state of stress is not easily predicted or is known to be approximately equal in all directions, such as structural

*Author to whom correspondence should be addressed. E-mail: feraboli@u.washington.edu
Figures 1–8, 10–13, 15–23, 25 and 28–33 appear in color online: <http://jrp.sagepub.com>

fittings, significant cost and weight savings can be achieved with the use of discontinuous fiber molding compounds for medium or large volume production. For such applications, unidirectional composite prepreg cannot be employed in an economically advantageous way due to its labor-intensive nature and poor ability to be draped over complex contours. Machined aluminum parts can be economically viable to produce, but are not compatible with carbon-fiber intensive airframes and lead to heavier designs. With rare exceptions, titanium castings cannot be used competitively because of the high casting factors, while titanium forgings rarely offer an economic advantage due to material waste and machining costs. The interest of the aerospace community for short fiber composites dates back to the 1960s and the pioneering work of Halpin, Pagano, and Kardos [4–8]. Furthermore, sheet molding compounds (SMC), secondary and tertiary airframe structures for non-interior applications have been in service for several years. SMC are typically used in conjunction with traditional compression molding, which we can identify as high-flow molding due to the large amount of resin flow and associated fiber orientation. SMC commonly feature 1.0 in. (25.4 mm) long glass fiber reinforcements and less 30–50% fibers by volume. Although their lower mechanical properties has traditionally limited their airframe applications, relatively large structures such as engine strut fairings have been in service for several years. In order to become attractive for more significant secondary as well as primary structures, higher performance fiber, resins and manufacturing methods are required.

This study investigates the behavior of a high-performance system that uses discontinuous carbon fiber/epoxy obtained from high-grade prepreg. Prepreg-based discontinuous systems are appealing for primary structural applications as they can be used in low-flow molding conditions, whereby minimal flow and reinforcement redistribution occurs upon molding. Commercial applications for this type of material form already exist, although using different resin systems and fiber types and lengths, under various manufacturers and denominations (e.g., Quantum Lytex 4149 and Hexcel HexMC [9,10]). Hexcel HexMC is used on the Boeing 787 Dreamliner for manufacturing the first composite structural window frame for a commercial airliner application [13]. The compression-molded composite window frames allow for significant weight saving and superior damage tolerance compared to a traditional aluminum frame.

MATERIAL FABRICATION AND TEST SET-UP

Material Fabrication

Discontinuous carbon/epoxy panels are manufactured in the laboratory starting from a TORAYCA T700/2510 unidirectional (UD) prepreg. The system is a 270°F cure (132°C), designated for vacuum oven cure of General Aviation airframe primary structures, and has a resin content of 36%.

In order to obtain a 10 in. × 10 in. (254 mm × 254 mm) discontinuous laminate, the required number of UD prepreg sheets is cut from the roll, as if to be used to generate a continuous fiber laminate. This procedure ensures that the correct amount of material is used, in a fashion similar to the weighing of the charge for SMC molding. Only one ply at a time is cut while the others are stored in the freezer to avoid tacking of the resin and reducing the formation of moisture. Each ply is clamped down (Figure 1) at one end with a purpose-built jig, and cut into 10 in. (254 mm) long and desired width. While clamped, each strip is cut into chips (or ribbons) of desired length. Chip lengths investigated are 0.5, 1.0, 1.5, 2.0, and 3.0 in. (12.7, 25.4, 38.1, 50.8, and 76.2 mm), while chip widths are 0.33 and

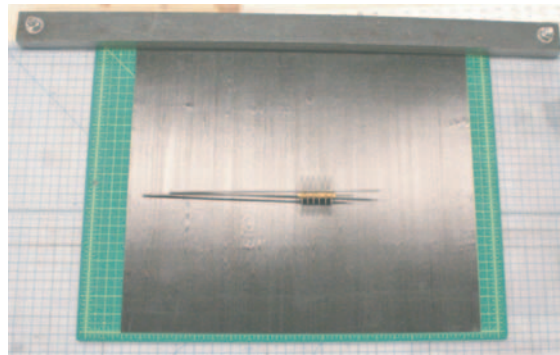


Figure 1. Cutting tool and clamping fixture used to perform the longitudinal slitting and transverse chipping of the prepreg.

Table 1. Global test matrix for this study.

ID	Family	Chip length <i>l</i> in.	Chip width <i>w</i> in.	Chip thickn. <i>t</i> in.	Aspect ratio <i>l/w</i>	Aspect ratio <i>l/t</i>	Orientation degrees	Thickn. in.	ASTM test	Test type	No. tests
1	A	0.5	0.33	0.005	1.5	100	0	0.071	D 3039	Tension	3
2	A	1.0	0.33	0.005	3.0	200	0	0.069	D 3039	Tension	3
3	A	2.0	0.33	0.005	6.1	400	0	0.091	D 3039	Tension	8
4	A	3.0	0.33	0.005	9.1	600	0	0.081	D 3039	Tension	3
5	B	0.5	0.33	0.005	1.5	100	0	0.070	Mod D 695	Compr.	3
6	B	1.0	0.33	0.005	3.0	200	0	0.070	Mod D 695	Compr.	3
7	B	2.0	0.33	0.005	6.1	400	0	0.070	Mod D 695	Compr.	3
8	B	3.0	0.33	0.005	9.1	600	0	0.070	Mod D 695	Compr.	3
9	C	0.5	0.33	0.005	1.5	100	0	0.074	D 790	Flexure	3
10	C	1.0	0.33	0.005	3.0	200	0	0.070	D 790	Flexure	3
11	C	2.0	0.33	0.005	6.1	400	0	0.088	D 790	Flexure	3
12	C	3.0	0.33	0.005	9.1	600	0	0.080	D 790	Flexure	3
13	D	2.0	0.16	0.005	12.5	400	0	0.142	D 3039	Tension	3
14	D	1.0	0.16	0.005	6.3	200	0	0.099	D 3039	Tension	3
15	E	2.0	0.33	0.005	6.1	400	45	0.092	D 3039	Tension	3
16	E	2.0	0.33	0.005	6.1	400	90	0.091	D 3039	Tension	3
17	F	2.0	0.33	0.005	6.1	400	0	0.158	D 3039	Tension	3
18	F	2.0	0.33	0.005	6.1	400	0	0.233	D 3039	Tension	3
19	G	QI*	–	–	–	–	0	0.084	D 3039	Tension	3
20	G	QI*	–	–	–	–	0	0.070	Mod D 695	Compr.	3
21	G	QI*	–	–	–	–	0	0.085	D 790	Flexure	3
22	H	QI**	–	–	–	–	0	0.087	D 790	Flexure	3

The symbols * and ** indicate two different quasi-isotropic lay-ups: $[0/90/+45/-45]_{ns}$ and $[90_2/+45_2/-45_2/0_2]_s$ respectively.

0.17 in. (8.4 or 4.1 mm). Using various combinations of chip width and length enables the parametric investigation of chip aspect ration on the mechanical response of the system. Table 1 summarizes the global test matrix implemented in the study, with identification numbers for individual categories within broader families of specimens having similar characteristics. Configuration 3A refers to ID number 3, family A, and it corresponds to the reference configuration for all subsequent parametric studies.

After removal of the backing tape, the chips are then set into the freezer to maintain low viscosity and prevent premature curing. In order to obtain an in-plane random distribution,



Figure 2. Random distribution of prepreg chips before curing.

the chips are scattered into a tray and shuffled until visual randomization is achieved (Figure 2). The random stack of chips is then press molded in an aluminum tool for 1 h at 270°F (132°C) under 80 psi (0.55 MPa) of pressure. Three nominal thickness values are investigated: 0.08, 0.160, and 0.240 in (2, 4, and 6 mm); thickness variation between nominal and measured can be significant (see Table 1) due to the nature of the process. The reference thickness used for the majority of the specimens of this study is 0.08 in. (2 mm), which is the lowest value that can usually be successfully molded with similar systems, and corresponds to the thickness of an eight-ply quasi-isotropic tape lay-up.

As the cured plate is removed from the tool, it exhibits several areas of evident defects around the edges, which include both resin-rich and resin-starved spots and voids (Figure 3). Removing the peripheral portions of the plate by often more than 1.0 in. (25 mm) in every direction greatly reduces the effective panel area (Figure 4) from which test specimens (Figure 5) can be extracted. A typical micrographic picture of a molded panel is shown in Figure 6. With the use of image analysis software, which isolates different grayscale values, it is calculated that a typical panel exhibits 0.48% voids and 28% resin content, thus resulting in an approximate 8% resin loss from the original prepreg. It should be noted that for this type of material form and process combination, voids are observed in the form of resin-starved pockets, due to the inability of the resin to flow in all interstices before consolidation, rather than diffused porosity. These differ from the voids typically observed for autoclave-cured parts, which manifest as diffused porosity in the matrix.

Since published supplier data for this material system is obtained using the vacuum bag oven cure process, it is necessary to generate comparative values using the same press-molding pressure and temperature profiles. Continuous fiber quasi-isotropic $[0/90/+45/-45]_{ns}$ lay-ups are molded to obtain a reference value, or upper bound, for the quasi-isotropic properties to be expected from the discontinuous panels. In flexure, a quasi-isotropic $[90_2/+45_2/-45_2/0_2]_s$ lay-up is also tested to obtain a lower bound for this

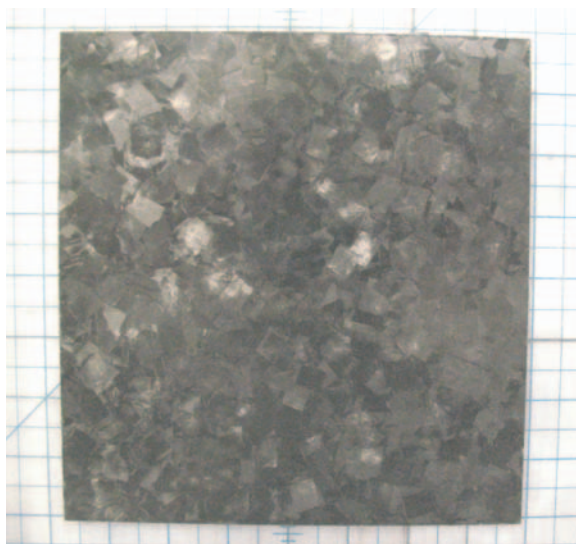


Figure 3. The laminate after cure, with machined edges.



Figure 4. Typical tensile test specimens with glass fiber/epoxy tabs.

kind of laminate. The higher pressures used in this study led to higher modulus and strength values than published ones.

It can be seen from Table 1 that a minimum of three specimens per test configuration (ID number) are tested, except for the baseline configuration 3A (ID 3, family A), where several more are tested. The large property variation typical of these materials would suggest testing several more specimens per configuration in order to build a statistically significant database. However, the complexity of manufacturing of these panels imposed a limitation on the amount of specimens that could be tested. All values reported in the following sections are the average over three specimens.

Test Set-up

Tensile, compressive and flexure tests are performed to investigate the influence of chip length. All specimens are loaded to failure at a rate of 0.05 in./min (1.3 mm/min) in a two-grip hydraulic tension/compression test frame. Tensile tests are performed in

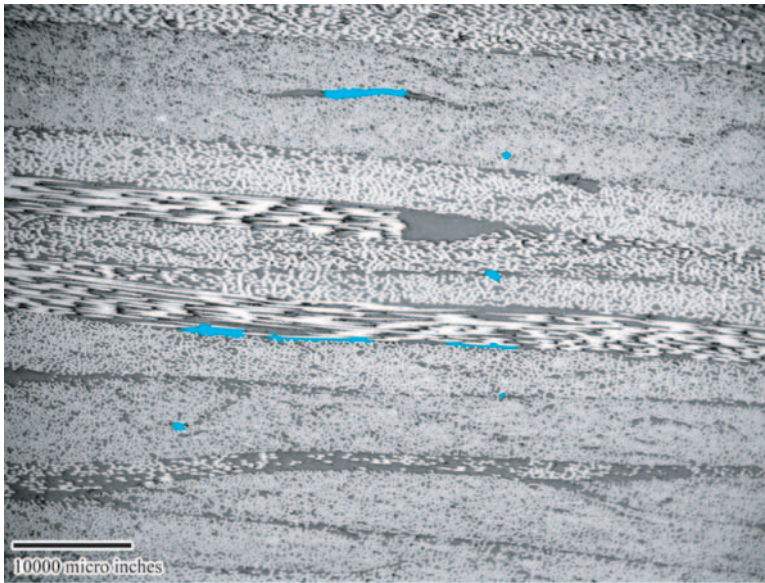


Figure 5. Micrographic cross-section exhibiting void content through image analysis.

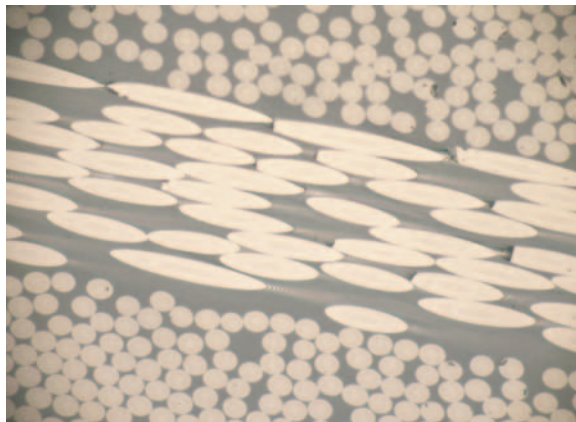


Figure 6. The degree of elliptical distortion of the fibers is an indicator of the chip orientation.

compliance with standard ASTM D3039 [17], using a 1 in. (25.4 mm) wide and approximately 8 in. (203 mm) long straight specimen. Longer specimens would have been desirable but it was not possible to obtain high quality areas from the molded panels that were longer than 10 in. Glass/epoxy tabs are bonded to the specimen using 3M Scotchweld film adhesive. Compressive tests are performed using the modified ASTM D695 standard [18]. Specimens 0.5 in. (12.7 mm) wide and 3.2 in. (81.3 mm) long are cut from each plate. The specimens are fitted with glass/epoxy tabs as prescribed by the standard. Flexure tests are performed in compliance with standard ASTM D790 [19]. All specimens are loaded to failure in three-point bending using a span of 2.0 in (50.8 mm), which gives a span to thickness ratio of 33, this is selected to accommodate all specimens due to minor variations in thickness. Specimen width is constant at 0.5 in. (12.7 mm).

For the present study, all strength data reported in the following sections refers to ultimate strength, calculated as the strength corresponding to ultimate load. Ultimate load is determined as the highest value of load reached in the load–displacement curve before a large drop, usually to values of half the previous ones.

For tensile and compressive tests, modulus is measured with an extensometer, while for flexure tests the modulus is calculated according to ASTM directions, as it cannot be easily measured.

Specimens are inspected post-mortem by cross-sectioning, polishing, and optical microscopy to characterize failure modes and morphology. A limited set of specimens, representative of A1–3 categories are machined and subject to resin burn-off and de-plying, to enable further inspection of the failure modes. Burn-off temperature (850°F or 454°C) and duration (3 h) are calibrated carefully in order to allow for partial resin burn-off (average weight loss is 25% per specimen, which leaves around 3% of resin content) while retaining sufficient chip integrity for subsequent de-plying.

RESULTS

Assessment of Random Distribution

Although the chips are randomized in the mold prior to curing, it is necessary to ensure that the process employed yields effectively in-plane isotropic distribution. Three methods are employed to estimate chip distribution, and to verify the effective random nature of the ‘laminate’:

- Image analysis of the cross-section to determine individual chip orientation through the thickness (destructive).
- Image analysis of the outer (top and bottom) surfaces of the panel (non-destructive).
- Testing of tensile specimens cut at 0, 45, and 90 degrees from the longitudinal axis (destructive).

All three methods successfully demonstrate the panels’ two-dimensional (in-plane) isotropic characteristic, yet each method however poses individual limitations to its applicability.

Image analysis of individual chips through the thickness is a destructive approach and requires careful analysis of the cross-section. Orientation of the chip is estimated based on the shape of the individual fibers: fiber aligned in the 0 direction exhibit a pseudo-circular section geometry, while fibers at 90 degrees appear as straight parallel bands (or are infinite ellipsoids, Figure 6). The degree of deviation from circular to elliptic geometry is a good indication of fiber orientation [14,15]. For small fiber angles, less than 20 degrees, it becomes very difficult to uniquely determine the effective orientation. Fibers at 0 and 20 degrees have nearly the same cross-sectional shape as the amount of elliptical distortion from the pseudo-circular shape is very small. To establish the direction of the orientation, as + and – fibers show the same elliptical shape, it is necessary to investigate the interference patterns associated to the carbon fiber underneath the thin layer of epoxy matrix. Focusing the lens in the neat resin surrounding the fiber at progressively increasing depths it is possible to detect the reflection of the shiny fiber below the opaque matrix [14]. In bright field analysis this phenomenon is partially visible (Figure 7, left), while in dark field the presence of the fiber becomes more apparent (Figure 7, right). While this method identifies uniquely the fiber orientation for fiber angles greater than 20–30 degrees, for

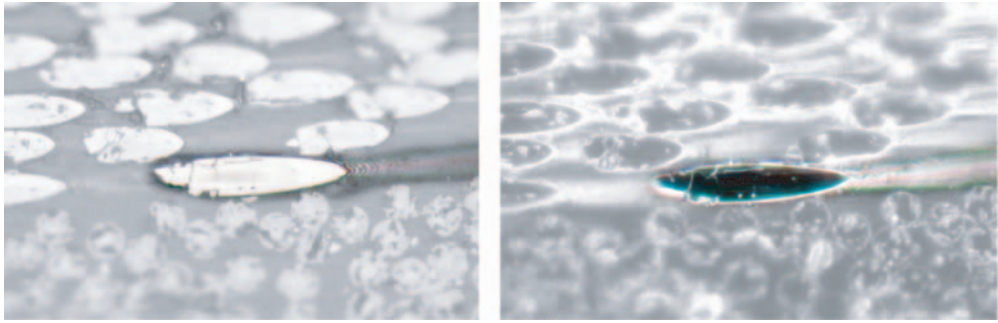


Figure 7. Bright field (left) and dark field (right) analyses show presence of fiber below surface, thus indicating the angle of orientation.

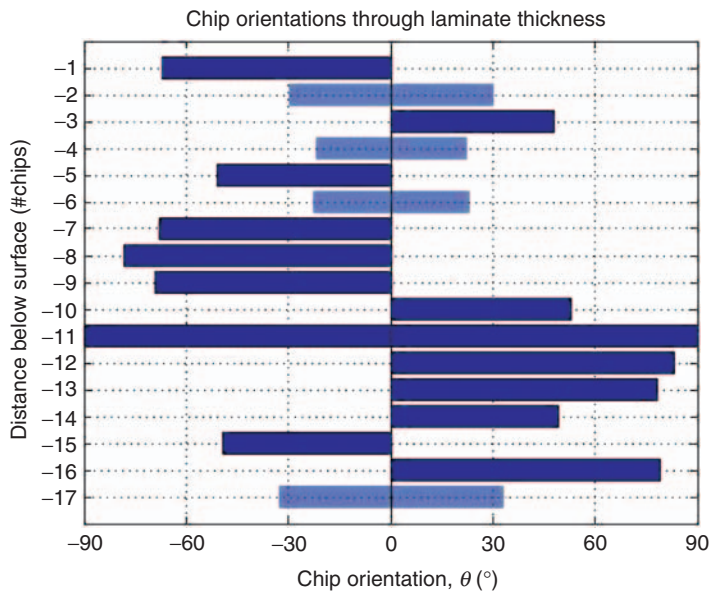


Figure 8. Typical visualization of chip distribution through the thickness shows quite even distribution along principal directions.

smaller fiber angles the amount of fiber visible below the surface is too small to be easily detected.

Based on these observations, it is possible to derive plots such as the one in Figure 8, which shows the calculated orientation of each of the 17 chips through the thickness, from the top surface of the 'laminate' downward. From the plot it can be seen that the distribution in the + and - directions as well as in the fiber orientations is relatively random, with a minor bias toward the high positive angles. Please note the absence of zero degree chips and the presence of four \pm 20-degree and 30-degree chips, for which it is not possible to uniquely identify the angle or orientation of the fibers.

Another method can be used to determine the orientation of the chips, and it offers the advantage of being non-destructive. However, it only allows for determining the orientation of the outer (visible) surfaces of a molded panel only, hence it is based on the

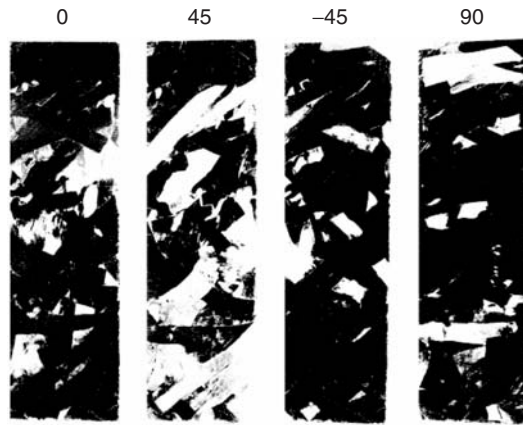


Figure 9. Images of a test coupon shot from four different angles and filtered to highlight contrast of chip reflection.

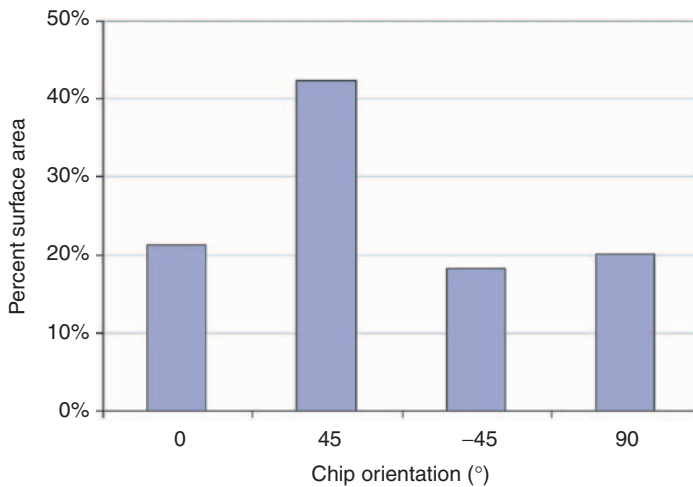


Figure 10. Percentage of fibers along the four principal directions of the specimens as calculated based on the image analysis of figure 26.

assumption that the external distribution is representative of the internal one [16]. Images of the panel or of a test coupon are shot from four different angles and then processed using a dark field filter. Taking advantage of the reflective characteristics of carbon fiber and opaque nature of epoxy, the orientation of the chips can be determined (Figure 9). Further accuracy could be obtained if images were to be taken from other angles, such as ± 22.5 degrees, and so on. Using image analysis software, the surface area corresponding to different grey tones (black and white) is calculated, thus giving the distribution such as the one in Figure 10. It can be seen that while 0 and 90 degree chips are present in nearly the same percentage, there is a bias in the +45 degree chips with respect to -45 degree ones.

A third and last method used to verify the quasi-isotropic nature of the tested panels is to machine tensile specimens in the 0, 45, and 90 directions from the assumed longitudinal

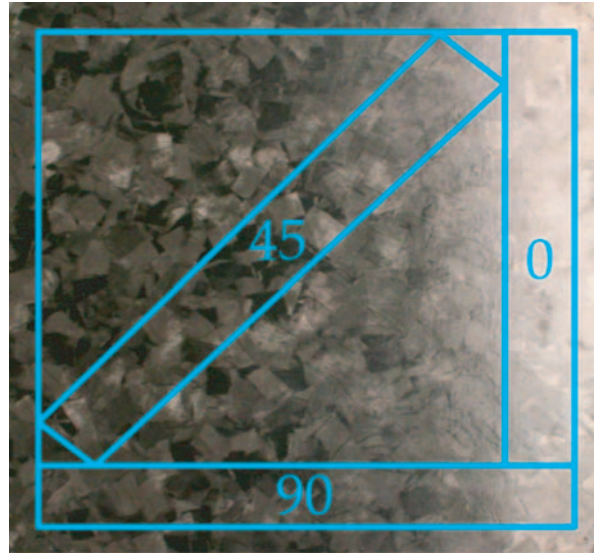


Figure 11. Example of coupons machined at different angles from the longitudinal axis.

direction of the molded panel (Figure 11) and to test them to failure. Results are shown in Figure 12, and show a 20% bias in the average ultimate strength between the 0 and the 90 degree values, while the 45 degree value is well in line with the 0 value. It should be kept in mind that only three off-axis specimens were tested to obtain these average strengths, and that given the high variation observed in these panels such observation is not conclusive. Yet, from all three methods it appears that there is an acceptable amount of repeatability in the process, and that although a random (non-repeatable) bias in a given direction may be present, the molded panels behave as in-plane isotropic.

Tension

Typical tensile load–displacement curves (Figure 13) appear to exhibit three kinds of behaviors following the initial linear range. The first kind, (A), sees the occurrence of one or more small drops in the curve, followed by one large final drop, indicative of catastrophic failure. The second kind, (B), is linear up to ultimate load, without preliminary small drops. The last kind, (C), sees the onset of ultimate load followed by a progressively decreasing (stepped) load bearing capability, less sudden than the previous two. Regardless of the shape of the curve, after reaching ultimate load, all specimens maintain a certain degree of integrity (Figure 14), without breaking in two halves. Failure occurs as ‘delaminations’ through the thickness in the form of separation of multiple chips in a single stack.

Micrographic pictures of Figure 15(a) and (b) show progressively closer views of a failed specimen. The specimen is locally divided in two fracture surfaces, which appear to have slid relative to each other. Multiple fracture fronts are visible through the specimen thickness, which indicate that fracture changes path longitudinally and transversely wherever it may be easier. It is interesting to observe that not a single chip, but rather a wedge consisting of several chips tends to pullout from the other half of the specimen.

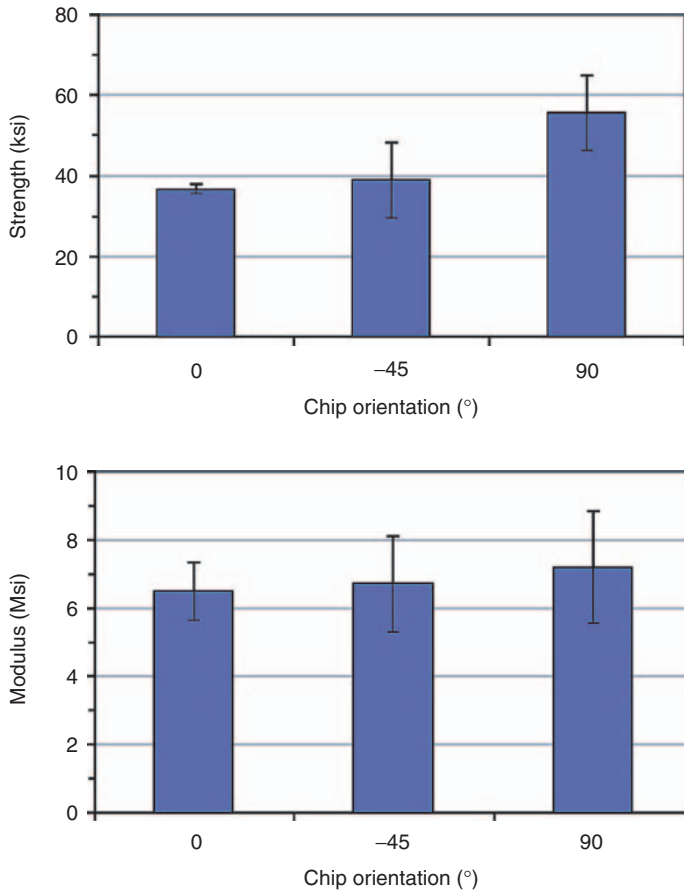


Figure 12. Tensile test results for panel used to verify degree of in-plane isotropy: ultimate strength (top), and modulus (bottom).

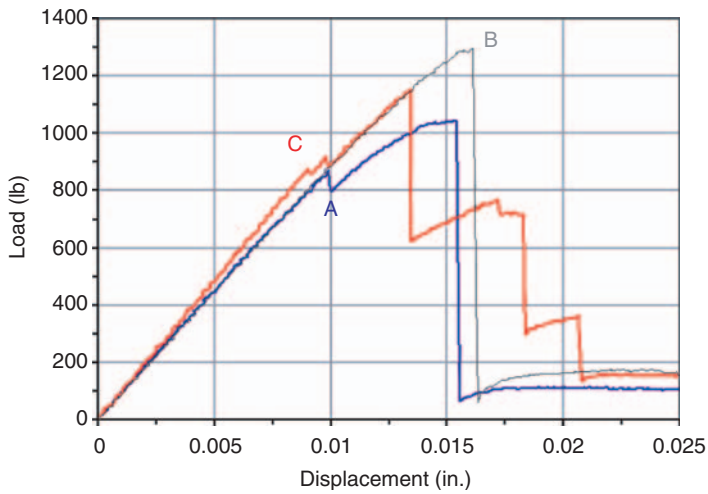


Figure 13. Typical tensile load-deflection curves observed show three different behaviors.

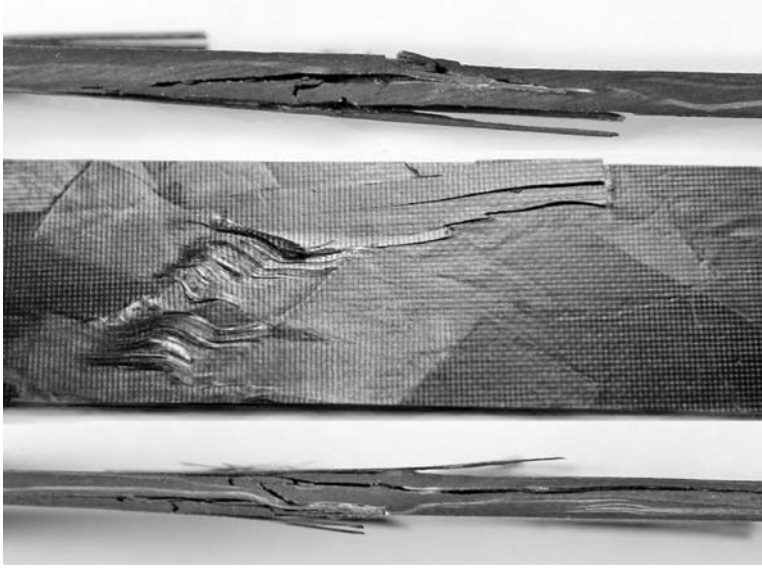


Figure 14. Typical morphology of tension failed specimen, top and side views.

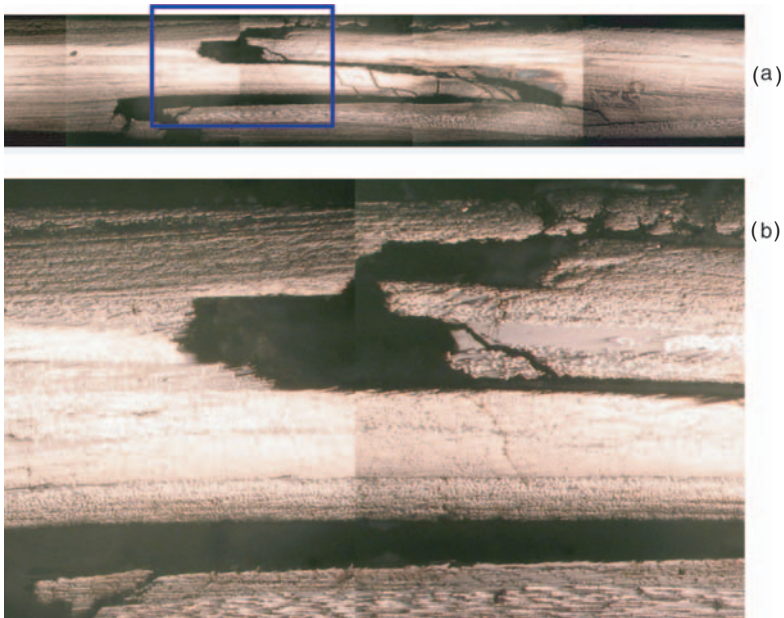


Figure 15(a, b). Sequence of micrographic pictures at increasing magnification for a typical tensile failure specimen.

The random orientation of the chips and of the individual fibers is clearly visible, as well as a large central resin-rich area.

A similar micrographic image (Figure 16(a)) highlights two distinct failure locations, one to the left, which resembles the one discussed before, and the other to the far right, which is the one shown in greater detail in Figure 16(b) and (c). The latter one is of interest

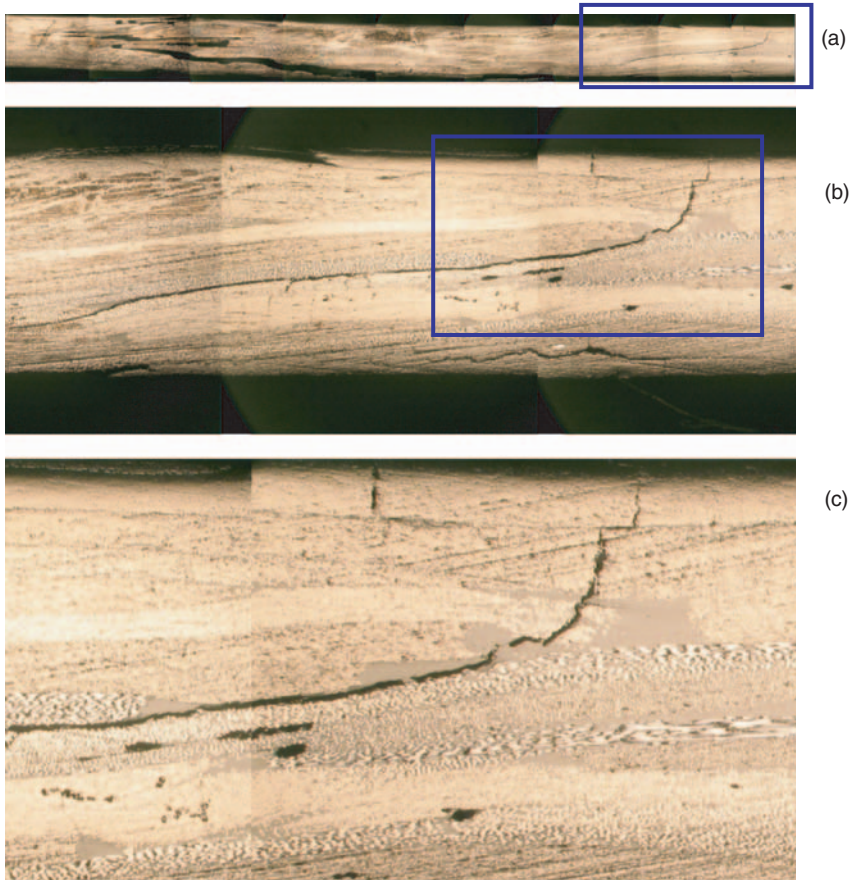


Figure 16(a–c). Sequence of micrographic pictures at increasing magnification of another typical tension failed specimen.

as it clearly highlights a combination of two failure modes between and within individual chips: cracking, or separation along a plane perpendicular to the chip axis, and ‘delamination’, or separation along a plane parallel to the chip’s length. Brittle fracture seems to start toward the surface, as tensile matrix failure, progress through a few chips, then eventually transform into delamination of one long chip from the remainder ‘laminare’. Counter-intuitively, the path of least resistance does not necessarily follow a resin-rich area (as shown in Figure 16(c)), a void, or a chip edge within the polished plane, since the neighboring chips (not visible) may offer different degrees of crack arrest.

From the tensile coupons, sections 3.0 in. (76 mm) long and centered on the failure location of the specimen are machined and subject to resin burn-off (Figure 17(a) and (b)). Due to the complex nature of the ‘laminare’, chips are removed individually where possible, or in small groups of 2–3 chips maximum if leftover resin does not allow for further separation. The specimen shown in Figure 17(c–e) is de-plyed progressively after the two partially fractured halves are delicately pulled apart (with minimal resistance). Subsequent stages of de-plying of one side of the fractured specimen reveal that failure occurs exclusively by chip disbonding and pull-off. The vast majority of the individual

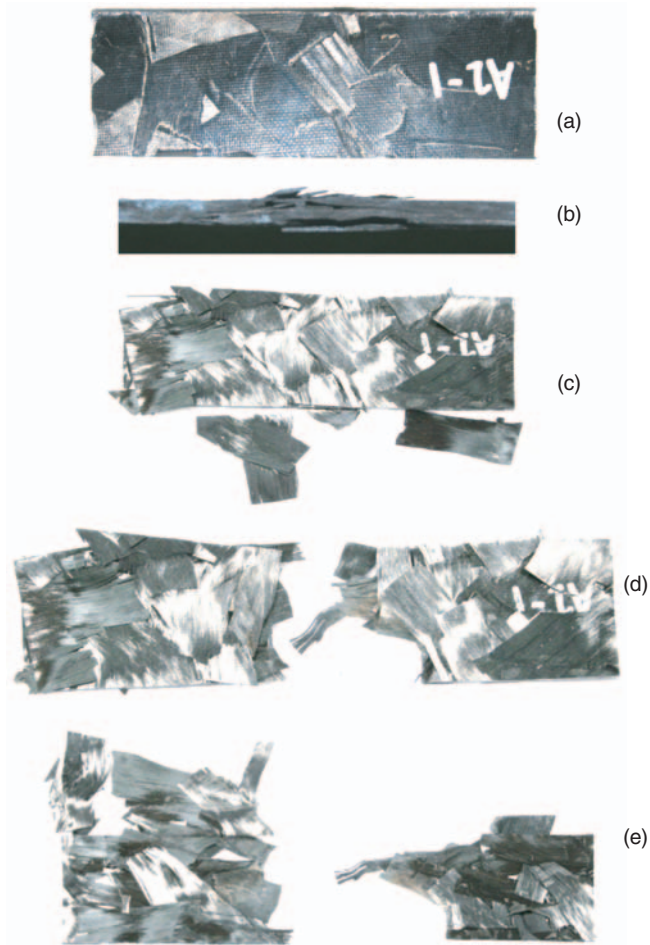


Figure 17(a–e). Pre-burn-off pictures from top (a) and side (b) and post burn-off de-plying after pulling the specimen apart along the fracture front (c–e).

chips remains intact, while some show distortion attributable to manufacturing or testing. However, little or no fiber breakage could be detected anywhere in the specimen.

Results for the ultimate strength and elastic modulus are plotted as a function of chip length in Figures 18 and 19 respectively. For reference, the average value of the continuous quasi-isotropic (QI) benchmark is also traced on the plot, without its associated variation bar. Ultimate tensile strength is shown to increase monotonically with chip length, but remains noticeably lower than the continuous QI value. On the other hand, modulus appears to increase negligibly in the range of chip lengths investigated, and overall virtually coincides with the QI reference value.

Compression

Typical compressive load–displacement curves (Figure 20) show the same three families of behavior as the tensile specimens. Independently of the shape of the curve, all specimens

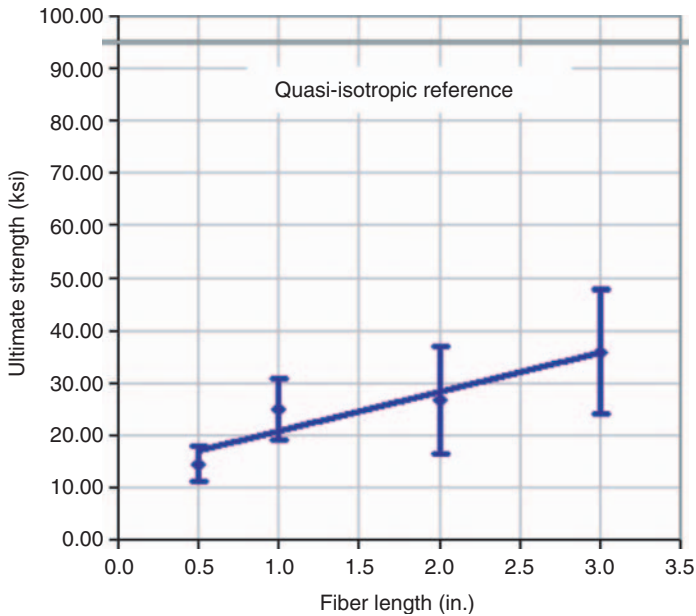


Figure 18. Average tensile ultimate strength plotted as function of chip length, with continuous fiber quasi-isotropic as reference.

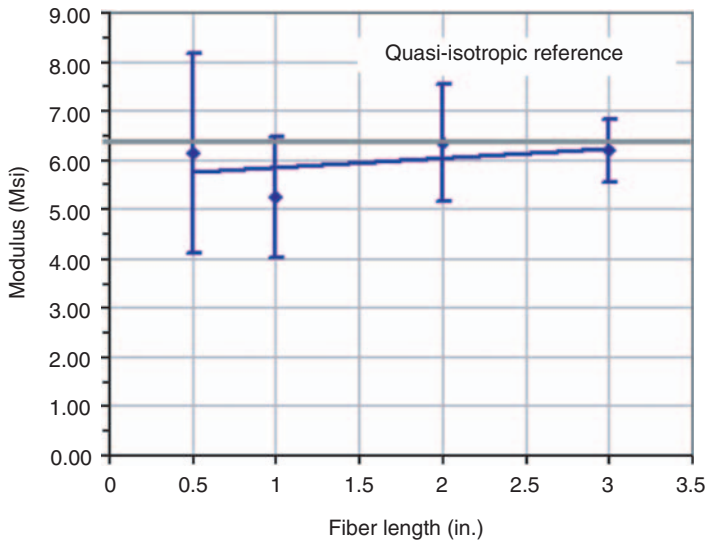


Figure 19. Average tensile modulus plotted as function of chip length, with continuous fiber quasi-isotropic as reference.

show good compression failure by fiber breakage, and ‘sublaminat’ separation. This separation is visible in Figure 21, where a wedge comprising several chips (similar to the tensile case) tends to slide into the other portion of the specimen. As in the tensile case, failure occurs by chip disbonding, followed by relative shearing rather than pullout, but does not involve extensive fiber buckling typical of compressive failure for continuous fibers.

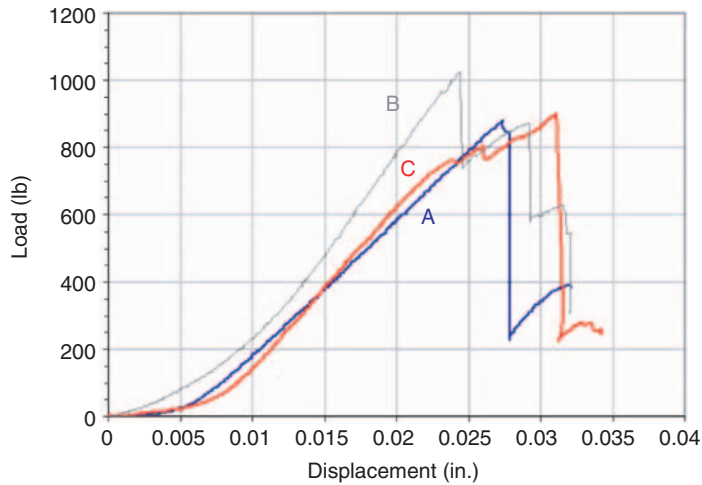


Figure 20. Typical compressive load–deflection curves observed show three different behaviors.

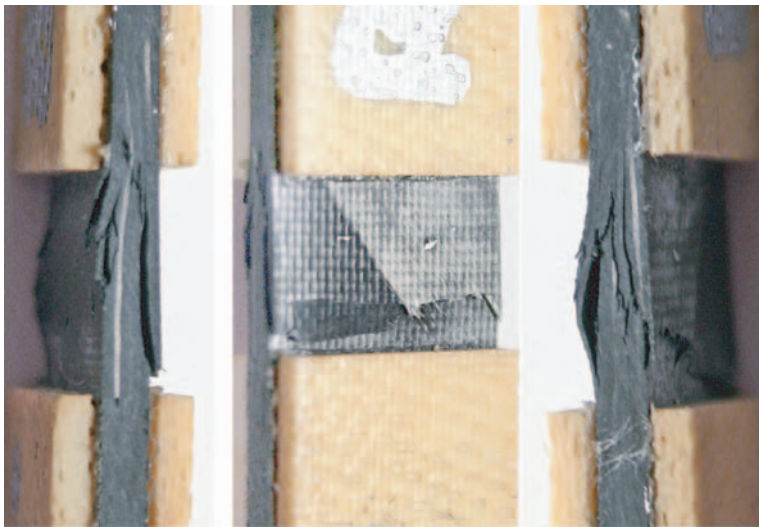


Figure 21. Typical morphology of tension failed specimen, top and side views.

Ultimate strength and modulus results are plotted against chip length in Figures 22 and 23 respectively. Similar trends to the tension case can be seen in both plots, however the ultimate strength in compression is closer to the QI value than in tension. Furthermore, modulus seems to increase more markedly between the shorter and longer reinforcements tested.

Flexure

Typical load–displacement curves for a flexure test are shown in Figure 24. For the shorter chip lengths, the curves tend to exhibit a less linear behavior than for the

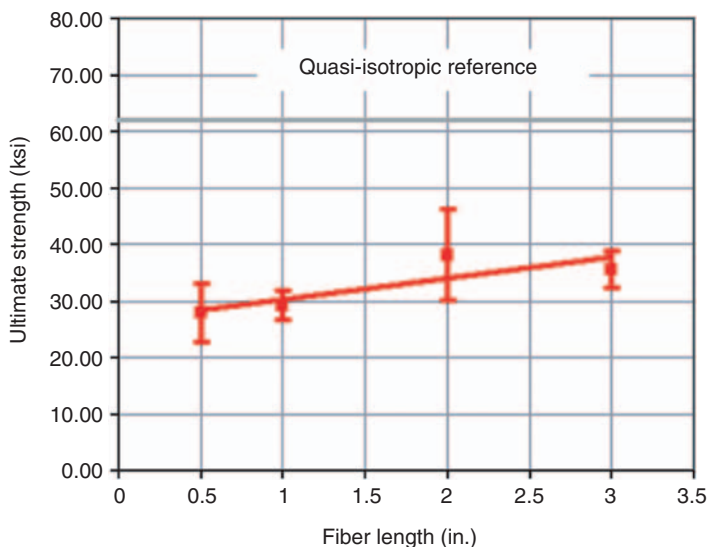


Figure 22. Average compressive ultimate strength plotted as function of chip length, with continuous fiber quasi-isotropic as reference.

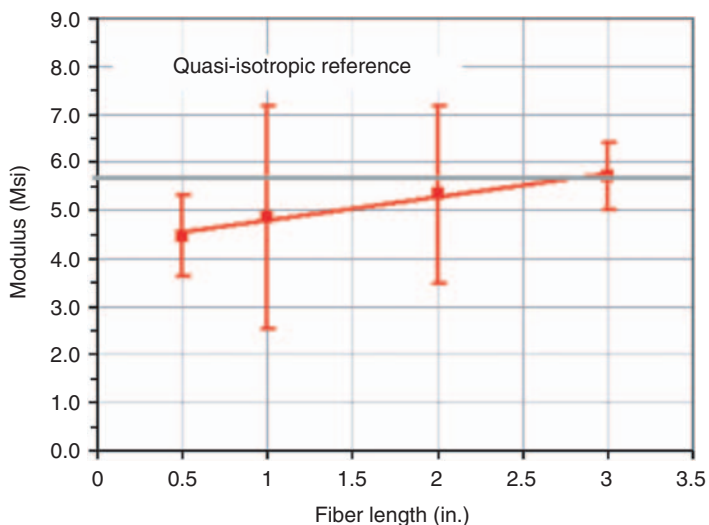


Figure 23. Average compressive modulus plotted as function of chip length, with continuous fiber quasi-isotropic as reference.

longer chips. Specimens fail in tension on the bottom surface, and exhibit chip disbonding and separation at such surface (Figure 25).

Ultimate strength and modulus results as function of chip length are shown in Figures 26 and 27. The effect of fiber length appears to markedly influence strength values, while modulus appears to be less affected. It should be noted that flexure modulus and strength for the discontinuous fiber exceed the values of the more compliant QI reference (category 23 H in Table 1), but are greatly inferior to the more performing QI reference (category 22 G in Table 1).

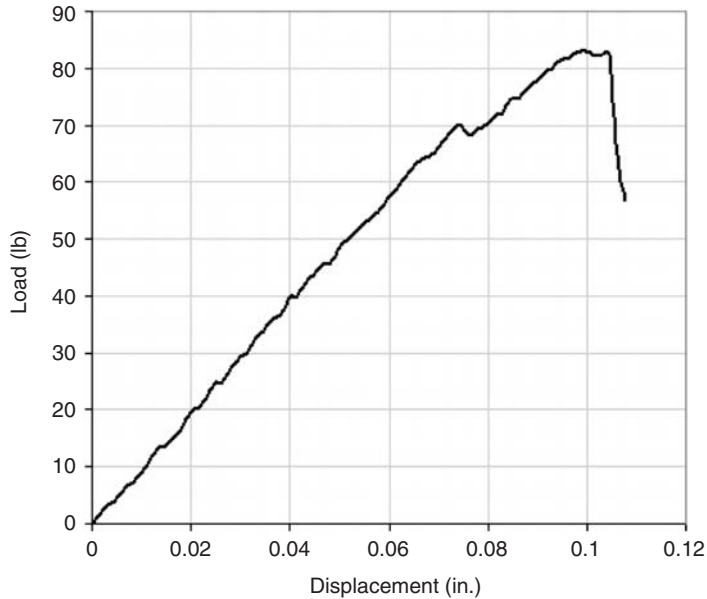


Figure 24. Typical flexural load–deflection curve.



Figure 25. Flexure specimen failing in tension directly below the loading roller.

DISCUSSION ON CHIP LENGTH AND ASPECT RATIO

The trends observed in Figures 18, 22, and 26 for tension, compression, and flexure strengths, respectively, are summarized in Figure 28. It is evident that average strength increases monotonically as a function of chip length. The longest chip specimens exhibit average strengths between 1.3 and 2.2 times larger than the shortest chip specimens, according to the loading case. Flexural strength is consistently the highest, followed by compressive and tensile strengths respectively. This behavior differs from continuous fiber laminates, such as the QI tested in this study, where compressive strength is always lowest, and tensile and flexural strengths are usually closer in magnitude. In general, ultimate strength is noticeably lower than quasi-isotropic continuous baseline. For all load scenarios investigated, the discontinuous systems perform almost equally well as the

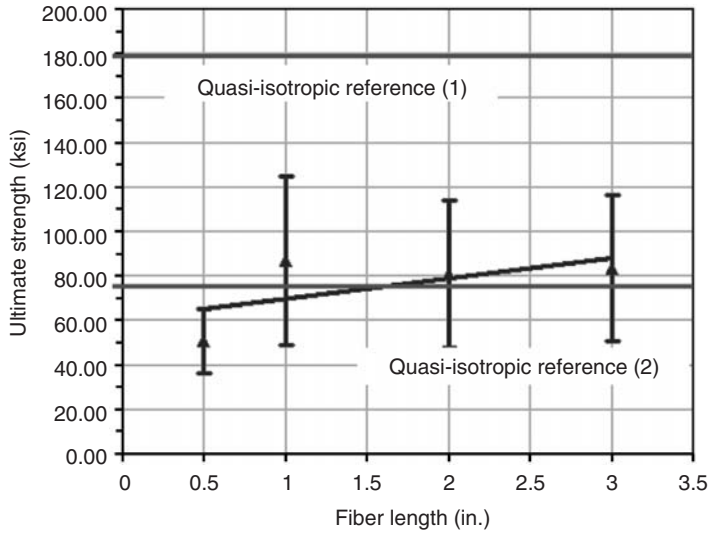


Figure 26. Average flexure ultimate strength plotted as function of chip length, with continuous fiber quasi-isotropic as reference.

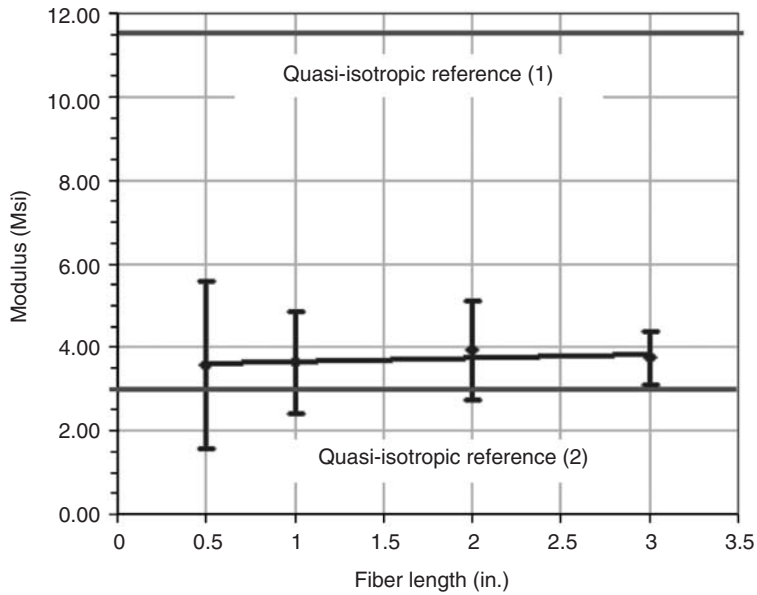


Figure 27. Average flexure modulus plotted as function of chip length, with continuous fiber quasi-isotropic as reference.

continuous quasi-isotropic benchmark from a stiffness standpoint, and across all chip lengths.

In a similar fashion to the previous plot, Figure 29 summarizes the trends observed in Figures 19, 23, and 27 for tension, compression, and flexure moduli, respectively. Although modulus appears to increase monotonically with respect to fiber length, the trends are much less defined than for strength. With the exception of compression, where

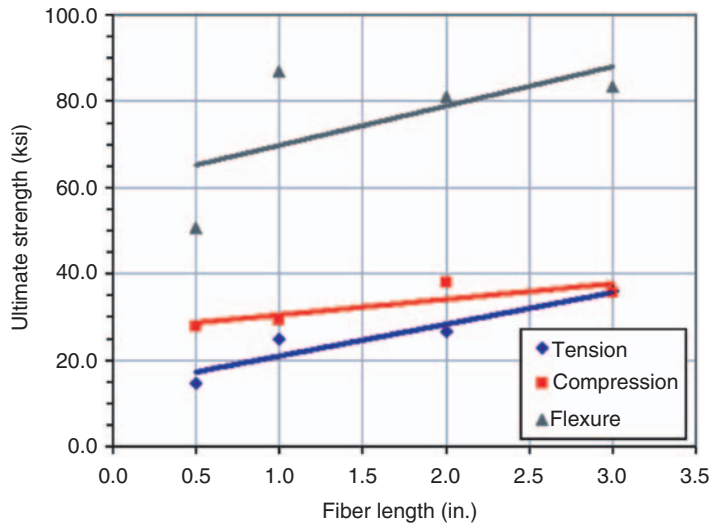


Figure 28. Tensile, compressive, and flexural ultimate strengths as function of chip length.

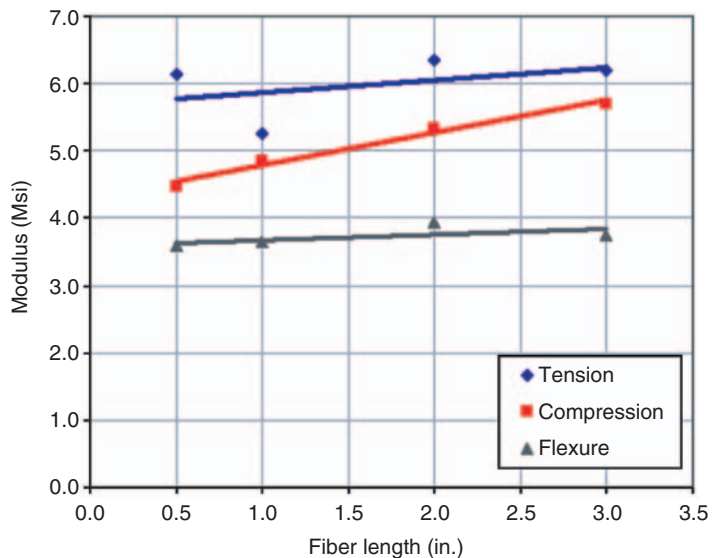


Figure 29. Tensile, compressive, and flexural moduli as function of chip length.

the longest chip is approximately 20% stiffer than the shortest one, tensile and flexural moduli are nearly constant for all chip lengths investigated.

From a mechanical performance standpoint, and limited to the number of specimens and specimen geometries tested, results seem to recommend the use of longer chips. However, longer chips add manufacturing complexities due to the greater possibility for fiber distortion/kinking, resin-rich or resin-starved areas and voids. The tradeoffs between manufacturing characteristics (drapeability, flow, etc.) and mechanical performance need to be further studied, and may lead to the determination of a compromise chip size.

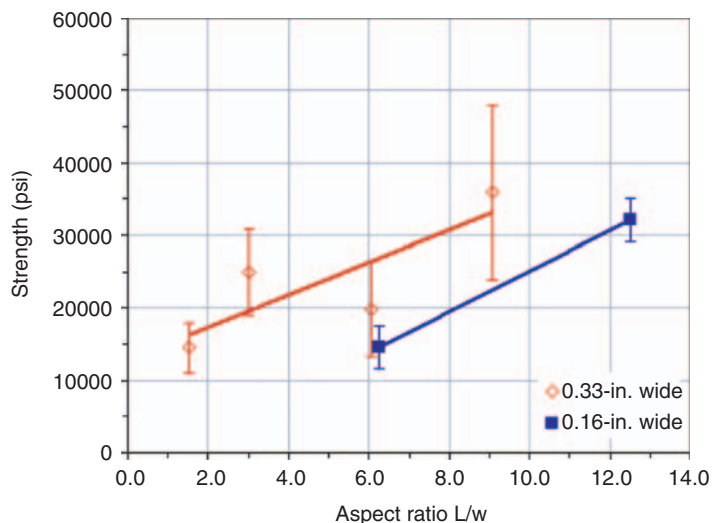


Figure 30. Tensile strength vs Aspect ratio for various chip lengths and widths.

Noticeable variation in the data was observed, ranging from 8% to 43% according to the loading conditions and specific property measured. However, it should be considered that the manufacturing process used in this study was not industrialized and that existing or future commercial systems will inevitably show reduced variation in the mechanical properties. Automated chip randomization and stacking will lead to improved mold coverage and reduced material waste, as well as less possibilities for contamination and moisture formation during the lengthy process of slitting and chipping. The use of more suitable resin systems, with *ad hoc* developed cure temperature, pressure and time, will also generate more flow in the matrix and thus lead to improved mold coverage and reduced void content.

Traditional discontinuous fiber theories [4–6], used in conjunction with SMC and P4 material forms, have made use of the fiber aspect ratio as the ratio of fiber length to fiber diameter (l/d). Since the load transfer between the fiber and the matrix occurs by shear, the critical aspect ratio [4] defines the transition between failure by fiber pullout (matrix failure) and failure by fiber breakage (fiber failure). For ribbon (flake) reinforced discontinuous systems, where the reinforcement has the form of a chip rather than an individual fiber, it has been suggested to use a modified aspect ratio that employs the chip thickness [7] or tow width [11,12].

By varying the width of the chip in conjunction with its length, it is possible to isolate the effect of aspect ratio on elastic response and failure initiation. For the present system, the ratio of chip length (l) to chip thickness (t) as well as chip width (w) has been used. The critical aspect ratio for this material system has been calculated to be 86, and its aspect ratio varies between 1.5 and 9.1 if the l/w ratio is used, and between 100 and 600 if the l/t ratio is used (see Table 1). The failure modes encountered suggest that complete shear transfer does not occur, thus for the chip sizes investigated the aspect ratio to be used is l/w rather than l/t . Tensile strength and modulus are plotted against aspect ratio in Figures 30 and 31 and show that strength greatly increases with such parameter, while modulus is relatively independent of it. It should also be noted that for the same l/w ratio, chips of larger width exhibit greater strength than those of smaller widths, while modulus seems to

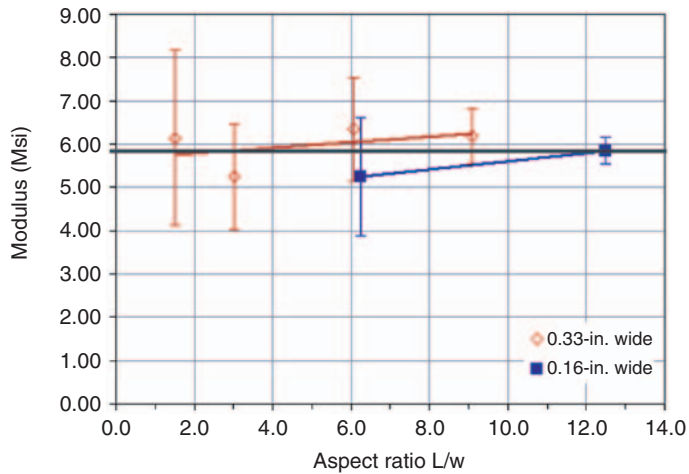


Figure 31. Tensile modulus vs aspect ratio for various chip lengths and widths.

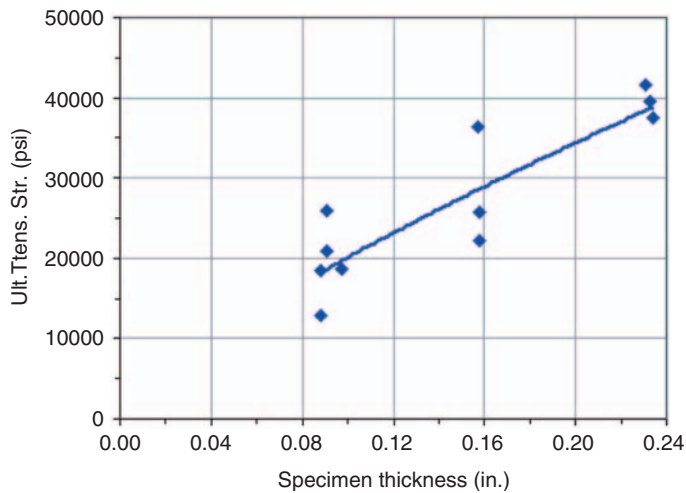


Figure 32. Thickness dependence of average ultimate tensile strength.

be independent again. Although not immediate, such observation is similar to others made in Ref. [10], which showed complex interactions between chip width and mechanical performance.

Thickness Effects

Another last important observation is that tensile strength as well as modulus are strongly dependent on molded plate thickness. Average ultimate tensile strength doubles between the 0.08 in. (2 mm) and the 0.24 in. (6 mm) panel thickness (Figure 32), and similarly average modulus increases by 50% between those two extremes (Figure 33).

The present study focused on a reference molded thickness of 0.08 in (2 mm) as it requires less material and effort to obtain given the lengthy and complex job of slitting and chipping prepreg. However, the strong dependence of elastic properties and strength on

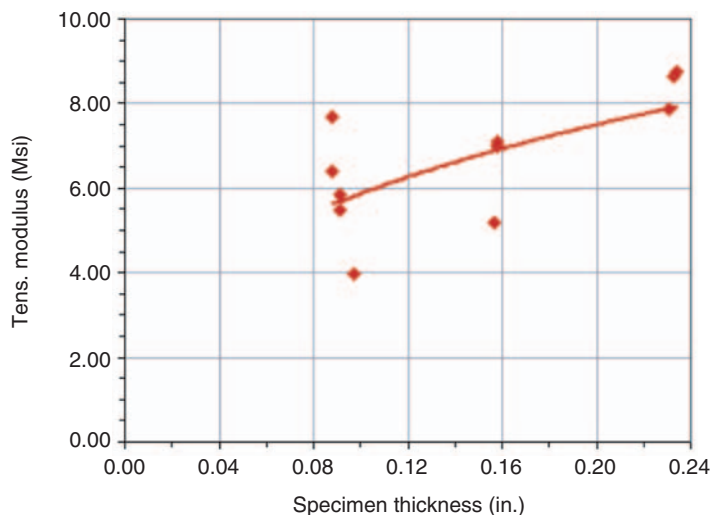


Figure 33. Thickness dependence of average tensile modulus.

panel thickness suggests that the heterogeneous nature of this material form may dictate the minimum gage requirements for successful molding. It is likely that bulk averaging of the properties may occur only for thicker panels, and that for those this kind of material form may exhibit the greatest potential benefits.

CONCLUSIONS

Flat plates have been press-molded successfully using discontinuous carbon fiber/epoxy prepreg chips and showed a satisfactory degree of randomization. Noticeable variation in the data was observed according to the loading conditions and specific property measured. Several chip aspect ratios were investigated and show a strong dependence of strength, more so than modulus, on chip aspect ratio. Failure is a matrix-dominated event, which occurs by transverse chip cracking, longitudinal chip splitting, and chip disbonding, with little or no fiber breakage. The failure path seems to be independent of location of voids and resin rich areas, possibly due to complex two-dimensional chip interactions. In general, ultimate strength is noticeably lower than quasi-isotropic continuous baseline, tensile strength being the weakest, followed by compression and flexure. For all load scenarios investigated, the discontinuous system exhibits moduli as high as the continuous quasi-isotropic benchmark and across all chip lengths. Its use for stiffness-dominated structural components may yield manufacturing advantages compared to equivalent continuous tape forms. A strong thickness dependence of strength and modulus may limit the minimum thickness that can be successfully molded.

ACKNOWLEDGMENTS

The authors wish to acknowledge Dr. Alan Miller (Director, Boeing 787 Technology Integration) for supporting this study. The contributions of Dr. John Halpin and Dr. Michael Graves are also gratefully acknowledged. The donation of prepreg material

by Andrea Dorr (Toray Composites of America) was fundamental for performing the study.

REFERENCES

1. Miller, A. G. (2007). The Boeing 787 Dreamliner, Keynote Address, *48th AIAA/ASME/ASCE/AHS/ASC Structures, Structural Dynamics, and Materials Conference*, Waikiki, HI, USA.
2. Stickler, P. B. (2002). Composite Materials for Commercial Transport – Issues and Future Research Directions, In: *Proceedings of the ASC, 17th Annual Technical Conference*, West Lafayette, IN, USA.
3. Ilcewicz, L. B., Smith, P. J., Hanson, C. T., Walker, T. H., Metschan, T. L., Mabson, G. E., Willden, K. S., Flynn, B. W., Scholz, D. B., Polland, D. R., Fredrikson, H. G., Olson, J. T. and Backman, B. F. (1997). Advanced Technology Composite Fuselage – Program Overview, NASA CR4734, April 1997.
4. Halpin, J. C. (1969). Stiffness and Expansion Estimates for Oriented Short Fiber Composites, *Polymer Engineering and Science*, **3**: 732.
5. Halpin, J. C. and Pagano, N. J. (1969). The Laminate Approx. for Randomly Oriented Short Fiber Composites, *Polymer Engineering and Science*, **3**: 720.
6. Halpin, J. C. and Kardos, J. L. (1978). Strength of Discontinuous Reinforced Composites, *Polymer Engineering and Science*, **18**(6): 496.
7. Kardos, J. L., Michno, M. J. and Duffy, T. A. (1974). Investigation of High Performance Short Fiber Reinforced Plastics, Final Report, Naval Air Systems Command, No. N00019-73-C-0358.
8. Giurgiutiu, V. and Reifsnider, K. L. (1994). Development of Strength Theories for Random Fiber Composites, *Journal of Composites Technology and Research*, **16**(2): 103–114.
9. Porter, J. (2004). Moving Closer to the Goal of Cost Effective Complex Geometry Carbon Composite Parts, HPC4HPC Special Session, *Proceedings of the 19th ASC Technical Conference*, Atlanta, GA, USA, Sept. 2004.
10. Starbuck, J. M., Jacob, G. C. and Simunovic, S. (2004). Energy Absorption in Chopped Carbon Fiber Compression Molded Composites, *Proceedings of the 16th ASC Technical Conference*, 2001, Also in Automotive Light-weighting Materials, Department of Energy, FY 2004 Progress Report. Chapters 4 and 5.
11. Harper, L. T., Turner, T. A., Warrior, N. A. and Rudd, C. D. (2006). Characterization of Random Carbon Fibre Composites from a Directed Fibre Preforming Process: The Effect of Fibre Length, *Composite Part A*, **37**(11): 1863–1878.
12. Harper, L. T., Turner, T. A., Warrior, N. A., Dahl, J. S. and Rudd, C. D. (2006). Characterisation of Random Carbon Fibre Composites from a Directed Fibre Preforming Process: Analysis of Microstructural Parameters, *Composite Part A*, **37**(11): 2136–2147.
13. Boeing 787 Features Composite Window Frames, Reinforced Plastics, *Application News*, Vol. 51, Issue 3, March 2007, Page 4.
14. Kawamura, M., Ikeda, S., Morita, S. and Sanomura, Y. (2005). Unambiguous Determination of 3D Fiber Orientation Distribution in Thermoplastic Composites using SAM Image of Elliptical Mark and Interference Fringe, *Journal of Composite Materials*, **39**(4): 287–299.
15. Zak, G., Park, C. B. and Benhaib, B. (2004). Estimation of Three-dimensional Fibre Orientation Distribution in Short-fibre Composites by a Two-section Method, *Journal of Composite Materials*, **35**(4): 316–339.
16. Nishimura, T., Ansell, M. P. and Ando, N. (2001). The Relationship Between the Arrangement of Wood Strands at the Surface of OSB and the Modulus of Rupture Determined by Mage Analysis, *Wood Science and Technology*, **35**: 555–562.
17. ASTM D3039/D3039M-00, Standard Test Method for Tensile Properties of Polymer Matrix Composite Materials, Volume 15.03, 2006.
18. ASTM D695-02a, Standard Test Method for Compressive Properties of Rigid Plastics, Volume 08.01, 2002.
19. ASTM D790-03, Standard Test Methods for Flexural Properties of Unreinforced and Reinforced Plastics and Electrical Insulating Materials, Volume 08.01, 2003.